Thermochemical characterization of polybenzimidazole with and without nano-ZrO$_2$ for ablative materials application

L. Paglia[1] · V. Genova[1] · M. P. Bracciale[1] · C. Bartuli[1] · F. Marra[1] · M. Natali[2] · G. Pulci[1]

Abstract

During the ballistic atmospheric re-entry, a space vehicle has to withstand huge thermo-mechanical solicitations because of its high velocity and the friction with the atmosphere. According to the kind of the re-entry mission, the heat fluxes can be very high (in the order of some MW m^{-2}) ;thus, an adequate thermal protection system is mandatory in order to preserve the structure of the vehicle, the payload and, for manned mission, the crew. Carbon phenolic ablators have been chosen for several missions because they are able to dissipate the incident heat flux very efficiently. Phenolic resin presents satisfying performance but also environmental drawbacks. Thus, a more environmental-friendly solution was conceived: a high-performance thermoplastic material, polybenzimidazole (PBI), was employed instead of phenolic resin. In this work PBI-ablative material samples were manufactured with and without the addition of nano-ZrO$_2$ and tested with an oxyacetylene flame. For comparison, some carbon-phenolic ablators with the same density were manufactured and tested too. Thermogravimetric analysis on PBI samples was carried out at different heating rates, and the obtained TG data were elaborated to evaluate the activation energy of PBI and nano-filled PBI. The thermokinetics results for PBI show an improvement in thermal stability due to the addition of nano-ZrO$_2$, while the oxyacetylene flame test enlightens how PBI ablators are able to overcome the carbon phenolic ablators performance, in particular when modified by the addition of nano-ZrO$_2$.

Keywords Polybenzimidazole · Ablative materials · Thermogravimetric analysis · Activation energy · Oxyacetylene flame exposure

Introduction

Ablative thermal shields have been used since the first Apollo mission and, after 50 years, they still represent the best choice for the ballistic atmospheric re-entry [1]. Among ablative materials, the light-weight ceramic ablators (LCA) have been selected for several missions because of their low density and high efficiency [2]. In particular, carbon phenolic ablators are composite materials consisting of a phenolic resin matrix and a carbon felt as reinforcing phase. An example is represented by PICA, and the carbon-phenolic ablator manufactured by NASA, and ASTERM, the European counterpart which is still in a developing phase. Carbon-phenolic ablative materials are unconventional composite materials consisting of a phenolic resin and a carbon felt. They have a very porous structure, and the quantity of phenolic resin has to be very low in order to preserve the lightness and the porosity of the final material [3–5]. The role of the phenolic resin is to improve the mechanical resistance of the carbon felt and to dissipate the heat by endothermic reactions of pyrolysis. In fact, when the phenolic resin reaches temperatures as high as 300 °C the pyrolysis becomes active and gaseous species and a porous carbonaceous residue are produced [6]. The gasses warm up absorbing part of the heat and, because of a pressure gradient, they flow through the porous char and go inside the boundary layer hindering the convective exchange between the material and the external heating flux (blockage effect) [7]. Because of all these phenomena, carbon-phenolic ablators were classified as semi-active insulating shield. The aim of this work is to propose a new polymer for this class of ablators, in particular a new

✉ L. Paglia
laura.paglia@uniroma1.it

1   Department of Chemical Engineering, Materials, Environment, INSTM Reference Laboratory for Engineering of Surface Treatments, Sapienza University of Rome, 00184 Rome, Italy

2   Civil and Environmental Engineering Department, University of Perugia, Strada di Pentima 4, 05100 Terni, Italy

polymer with a reduced environmental impact compared to the phenolic resin, but able to provide the same beneficial effects in terms of thermal protection. A promising candidate is the polybenzimidazole which is a thermoplastic polymer with exceptional thermal and chemical stability [8, 9]. Its glass transition temperature is very high and near to its temperature of decomposition, thus it does not show a melting point [10, 11]. PBI (polybenzimidazole) has been mainly used as electrolyte material for proton exchange membrane (PEM) fuel cells which operate under anhydrous conditions at high temperature (~ 200 °C). For this kind of application, it could be doped with phosphoric acid to improve its performance [12, 13] and, in other studies [14, 15], PBI was successfully modified by the addition of different compounds and also with inorganic fillers in order to increase its proton conductivity.

For its promising properties, PBI was selected for manufacturing an innovative ablator having carbon felt as reinforcing phase and PBI as matrix material. A new manufacturing strategy was elaborated for obtaining this composite material with a density of about 0.3 g cm^{-3}, comparable with the more traditional carbon-phenolic ablators [6, 16]. The thermal protection performance of the manufactured ablators was assessed by an oxyacetylene flame system [17] designed and engineered by the Laboratory of Surface Engineering and Materials of the Sapienza University of Rome [18].

Materials and methods

Matrices, reinforcement and nano-filler

Four different kinds of materials were manufactured for this work: two carbon phenolic ablators and two new ablators with PBI as polymer matrix. The carbon-phenolic ablative materials were manufactured with a commercial carbon felt (MFA Sigratherm, SGL Carbon) and a resole phenolic resin (Durite SC 1008) as described also in previous works [3, 19]. In addition to the standard material (denominated PhR) another one was manufactured with the addition of nanoparticles of ZrO_2 (denominated PhR-Z). PhR-Z ablators were obtained by adding 10 mass% of nano-ZrO_2 (50–100 nm) with respect to the final mass of cured resin. A final density of about 0.33 g cm^{-3} was obtained for each sample. For the other two kinds of PBI ablators, the same carbon felt (MFA Sigratherm) was employed as reinforcement. Also, in this case the ablator was manufactured with a final density of 0.33 g cm^{-3} and, a nano-filled ablator was proposed with 10 mass% of nano-ZrO_2.

PBI is a fully aromatic heterocyclic polymer (PBI structure shown in Fig. 1) characterized by an excellent mechanical and chemical stability. Its glass transition temperature (T_g) is about 450 °C [19, 20], while the initial decomposition
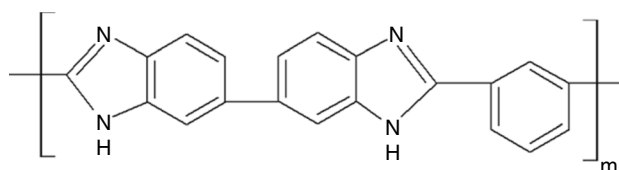

Fig. 1 Polybenzimidazole

temperature is very close to the T_g, for this reason PBI can be heated at high temperature, and it never melts or burns but decomposes [10, 21]. It is usually employed as fibers for high-performance protective apparels, aircraft wall fabrics, firefighter coats and suits, high-temperature protective gloves, protective clothing for pilots [11, 22], while as membrane it can be employed for proton exchange membrane in fuel cells because it allows for working at temperatures as high as 200 °C [8, 19, 23]. Furthermore two other materials were manufactured in order to have samples for the thermogravimetric analysis: a film of PBI polymer (PBI/m) and a film of PBI polymer enriched with 10 mass% nanoparticles of ZrO_2 (PBI/m-Z). The properties of the raw materials, as provided by the suppliers, are reported in Table 1, while the compositions of the manufactured materials are reported in Table 2.

Manufacturing procedure

Cylindrical samples of Sigratherm MFA were infiltrated with a solution of phenolic resin and ethylene glycol in a proportion suitable for obtaining the desired final density of 0.33 g cm^{-3}. The manufacturing process consists of several steps aiming at guaranteeing a good distribution of the phenolic resin inside the carbon felt, at ensuring a perfect crosslinking of the phenolic resin and optimizing the dispersion of the nano-filler inside the resin.

For PhR-Z samples, there is a preliminary step in which the desired amount of ceramic nanoparticles were mixed with the solvent and ultrasonicated for 2 h (Sonic Dismembrator model 505, Fischer Scientific), then the procedure is the same for PhR and PhR-Z.

At first, the solution of phenolic resin and ethylene glycol was ultrasonicated for 30 min and then heated on a stirring hot plate (IKA RTC basic) until an incipient phase of gel formation. A second phase of ultrasonication with the same parameters was proposed before the infiltration process. The solution was then poured inside a beaker where carbon felts were positioned inside a metal grill so that they cannot float and cannot lay at the bottom of the beaker where the stirrer continues to spin ensuring a continuous mixing of the solution during the heating. This phase ends when the gelification process is complete. At this point, the samples

Table 1 Raw materials properties according to suppliers data sheet

Phenolic resin	Solids ($T = 135$ °C)	60–64%
	Solvent	Isopropanol
	Free formaldehyde	0.6–0.2%
	Free phenol	11–18%
	pH ($T = 25$ °C)	7.0–8.5%
	Gel time ($T = 135$ °C)	11–18 min
	Colour	Golden yellow
Polybenzimidazole	Density	1.30 g cm^{-3}
	Glass transition temperature	427 °C
	Thermal conductivity	0.4 W m^{-1} K^{-1}
	Coefficient of linear thermal expansion (23–150 °C)	25×10^{-6} m m^{-1} K^{-1}
	Tensile stress at break	140 MPa
	Young modulus	5.8 GPa
Sigratherm MFA–carbon felt	Density	0.15 g cm^{-3}
	Thermal conductivity	0.22 W m^{-1} K^{-1}
	Young's modulus	0.25 GPa
	Bending strength	1.2 MPa
	Compression strength	0.9 MPa
ZrO₂	Granulometry	50–100 nm
	Density	5.7 g cm^{-3}
	Thermal conductivity	2.5 W m^{-1} K^{-1}
	Melting point	2680 °C

Table 2 Manufactured materials

Ablator	Description	
PhR	Matrix	Phenolic resin
	Reinforcement	MFA carbon felt
	Nano-filler	NO
PhR-Z	Matrix	Phenolic resin
	Reinforcement	MFA carbon felt
	Nano-filler	10 mass% ZrO₂ (particles 50–100 nm)
PBI	Matrix	PBI
	Reinforcement	MFA carbon felt
	Nano-filler	NO
PBI-Z	Matrix	PBI
	Reinforcement	MFA carbon felt
	Nano-filler	10 mass% ZrO₂ (particles 50–100 nm)
PBI/m	Matrix	PBI
	Reinforcement	NO
	Nano-filler	NO
PBI/m-Z	Matrix	PBI
	Reinforcement	NO
	Nano-filler	10 mass% ZrO₂ (particles 50–100 nm)

were removed from the gel and cured in a furnace at 180 °C for 24 h.

The traditional processing technique for thermoplastic polymers are not suitable for PBI because of its high T_g, but it exhibits solubility in some organic solvents, in particular in dimethylacetamide (DMAc) [19]. For these reasons, Celazole PBI powder was mixed with DMAc at the maximum allowed concentration (5 mass%). The solution was mixed and heated with a stirring hot plate at a temperature lower than 150 °C, in order to avoid the boiling, for a time of about 6 h obtaining a more concentrated solution. After this process, the solution was cooled down at 80 °C that is an operative temperature suitable for the ultrasound probe. At this stage, an ultrasonication of about 20 min guarantees an homogenization of the solution which can be filtrated and used to infiltrate the carbon felt samples (cylindrical samples with a diameter of 14 mm and a height of about 35 mm). The solution with the carbon felt samples inside was let on the stirring hot plate for other 2 h, and then it was let at room temperature for 24 h. After this period, the samples were got out from the very viscous solution of PBI and DMAc and cured in an oven at different temperatures: 110 °C for 3 h, 150 °C for 8 h, 200 °C for 12 h. This procedure was repeated also for samples of PBI-Z ablators, but in this case the nanoparticles of ZrO₂ were preliminary added to the DMAc and ultrasonicated for 2 h; then the suitable amount of PBI powder was added to the suspension and ultrasonicated for other 2 h to guarantee a satisfying dispersion of the nanoparticles. After this preliminary procedure, the manufacturing process can be repeated as in the previous case.

Thermogravimetric analysis and activation energy evaluation

Thermogravimetric analysis was carried out on polybenzimidazole at four different heating rate (2.5 °C min^{-1}, 5 °C min^{-1}, 7.5 °C min^{-1} and 10 °C min^{-1}) with a TG

analyzer (Q600, TA Instrument) in argon atmosphere. During the test, a continuous flux of 100 mL min^{-1} of argon guarantee the removal of pyrolysis gasses and so a constant atmospheric condition. The temperature during the test varies from RT to 1000 °C.

Tests were carried out on samples of PBI polymer (PBI/m) and PBI polymer with nanoparticles of ZrO_2 (PBI/m-Z) which were previously reduced to powder and divided with the quartering method for obtaining the desired mass of about 10 mg for each test.

The kinetics of decomposition of polybenzimidazole were not examined in depth in literature, thus for this study a traditional approach for the individuation of the steps of reaction and for the calculation of the activation energy was proposed: the number of steps of reaction corresponds to the number of peaks in the DTG curves of the materials [16, 24], while the activation energy was calculated according to the Friedman method with a commercial software for reaction kinetics analysis, AKTS-thermokinetics. As reported in the ICTAC recommendations [24], Friedman method is the most common differential isoconversion method; it does not require any numerical approximation and it is applicable to any temperature program [6, 24–28]. It was selected for this work because it is widespread for the evaluation of the decomposition kinetic parameters and the obtained results can be compared with the ones obtained by the authors in a previous work [6]. This method presents also some limits, for example inaccuracies can arise when the heat of reaction strongly depends on the heating rate or when the TG data are noisy and need to be smoothed for the elaboration [24].

AKTS-thermokinetics software was chosen to elaborate the TG data and to evaluate the apparent kinetic energy. This software uses the advanced differential isoconversional techniques for analysis and for predictions. With this strategy, the processes can be described combining parallel or consecutive steps because at each time point several elementary (usually unknown) processes take place simultaneously. Therefore, AKTS Software introduces the assumption of the existence of several reaction models necessary for the kinetic analysis of the investigated process. The software can provide as output the apparent activation energy calculated with several methods: Friedman, Ozawa–Flynn–Wall and according to the standard procedure of ASTM A698 [29].

The PBI polymer (*A*) pyrolysis produces a carbonaceous residue (*B*) and pyrolysis gas (*C*), so the reaction can be written as follows (Eq. 1).

$$A \rightarrow B + C \tag{1}$$

The kinetics of the reaction (Eq. 2) can be written considering k as the rate of variation of reagent and f a suitable function of *A* [30–32].

$$\frac{d[A]}{dt} = k \cdot f([A]) \tag{2}$$

The function $\alpha(t)$, called extend of reaction and ranging from 0 to 1, can be defined for expressing the quantity of reagent so that $\alpha(t) = 0$ at the beginning of the reaction and $\alpha(t) = 1$ at the end. $\alpha(t)$ is a function of time, but considering a constant heating rate $\beta = dT/dt$ it can be rewritten as a function of the temperature as shown in Eq. (3).

$$\alpha(T) = \frac{m_0 - m(T)}{m_0 - m_f} \tag{3}$$

where m_0 is the initial mass and m_f is the final mass when the reaction is complete. For the rate of the variation of reagent an Arrhenius law can be considered (E_a is the activation energy, A is the pre-exponential factor, R is the universal constant for perfect gas, T is the temperature), thus Eq. (2) can be rewritten as Eq. (4).

$$\frac{d\alpha(T)}{dT} = \frac{A}{\beta} f(\alpha) \cdot e^{-\frac{E_a}{RT}} \tag{4}$$

AKTS-Thermokinetics can elaborate the input of the TG curves at different heating rate to obtain the activation energy of the reaction according to the Friedman method [25, 33], which is a model free method consisting in applying the logarithmic derivative at the Eq. (4) obtaining Eq. (5), so that the activation E_a is proportional to the slope of the curve with $(-1/T)$ as abscissa and $\ln\left(\beta \frac{d\alpha}{dT}\right)$ as ordinate. Thus, for each extent of reaction α, the data of the four TG curves at different heating rates are used for calculating a value of E_a.

$$\ln\left(\beta \frac{d\alpha}{dT}\right) = \ln(f(\alpha)) + \ln A - \frac{E_a}{RT} \tag{5}$$

When a multi-step reaction is considered, the Friedman method can be applied to a single step of pyrolysis, thus there will be n step of pyrolysis and *n* values of activation energy E_a. In this case, there are also *n* extend of reaction functions $\alpha_i(T)$ with $i = 1, \ldots, n$ and a global extend of reaction expressed in Eq. (6).

$$\alpha_{TOT}(T) = \sum_{i=1}^{n} \alpha_i(T) \frac{W_{0i} - W_{fi}}{W_0 - W_f} \tag{6}$$

According to Friedman method, the activation energy for each step of reaction is proportional to the angular coefficient of the isoconversion curves. For each estimation of the angular coefficient (and so of E_a) AKTS software provides the value of the correlation factor r, which gives the goodness of the interpolation for the isoconversion curves.

Usually, at the beginning and at the end of each step of reaction, the value of r is always too low, but there is an

interval of α in which its value is high and near to 1. In this work only the activation energy values having a correlation factor higher than 0.99 were selected.

AKTS software needs to elaborate several TG curves with different heating rates (at least four) for obtaining the apparent activation energy. The software procedure consists of the smoothing of the TG curves, the definition of the baselines and the integral operation for obtaining the DTG curves. In this study, a multistep reaction is hypothesized thus, each step need to be treated separately: the DTG curve for each heating rate was deconvolved in three Gaussian functions. The four Gaussian functions for the first, second and third steps of reaction were used for the evaluation of the three apparent activation energies following the Friedman method as previously described. After each single evaluation, the software performs an optimization of the results and the goodness of the numerical values was enlighten by the correlation value r [29].

Oxyacetylene flame test

The oxyacetylene flame exposure test was carried out on the four kinds of ablators according to the ASTM standard E285/08 [12]. The facility for this test was designed and engineered by the Laboratory of Materials and Surface Engineering of Sapienza University of Rome and consists of an oxyacetylene burner able to deal with different flow rate of oxygen and acetylene, a two-color digital pyrometer (Impac Infrared, Frankfurt, Germany) for recording the temperature on the top of the exposed sample, a k-thermocouple for the temperature at the back of the sample, a heat flux sensor

Table 3 Oxyacetylene flame exposure parameters

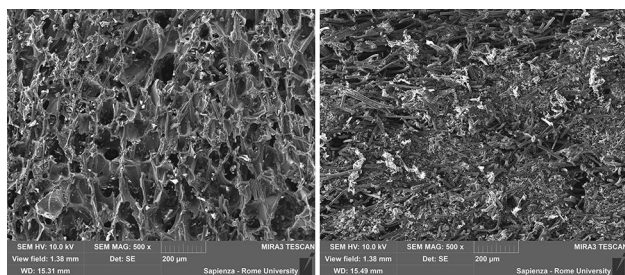|	Oxygen	Acetylene
Pressure/bar	2.5	0.3
Volumetric flow/NL h⁻¹	300	315

Fig. 2 Microstructure of a PhR sample (on the left) and of a PBI sample (on the right)

(HFM 1000 Vatell Corporation, Christiansburg, VA, USA) for measuring and calibrating the cold wall heat flux. All output data were monitored and recorded during the test by a data acquisition system (National Instrument), and LabView software was used to have a virtual interface for providing the input parameters to the system and monitoring and recording the output data during the test.

Three cylindrical samples (14.0 mm of diameter and 30.0 ± 0.2 mm of height) for each kind of material were exposed to oxyacetylene flame and volumetric flow rates of the gases were selected for obtaining neutral combustion conditions (tests parameters are summarized in Table 3). The samples were positioned in an insulating frame with a thickness of 10 mm to ensure the steadiness of the sample during the test. An heat flux of 4 MW m⁻² and an exposure time of 60 s were selected for the test. The k thermocouples measure the back temperature and were put always in the center of the sample and at 1 cm from the bottom thus setting a distance of 2 cm between the exposed surface of the sample and the thermocouple tip. At the end of the exposure, the samples were weighted and measured for evaluating the mass loss and the surface recession.

Results and discussion

Microstructural characterization

Several samples of PhR and PhR-Z ablators and PBI and PBI-Z ablators were cut along their axis and prepared for being observed with a scanning electron microscope (Tescan–Mira3). The micrographs in Fig. 2 show the distribution of the resin and of the polymer inside the felt: for PhR and PhR-Z samples the distribution is more homogeneous and the resin distributes in very thin layer among the fibers; PBI and PBI-Z show a cross section with areas at higher and at lower concentration of polymer. For every kind of ablator, the manufacturing process guarantees the same distribution of the phenolic resin or PBI inside the carbon felt both near the edge of the sample or in the inner part of it. Samples with the addition of nano-ZrO₂ were observed also to evaluate the goodness of the distribution and dispersion of the particles: in Fig. 3 SEM micrographs show the homogeneous distribution of the nano-filler inside the resin and BSE micrographs at higher magnification enlighten the good dispersion of nanoparticles within the resin with only few submicrometric agglomerates.

These results demonstrate that there is a good compatibility between the nanoparticles and the polymer (both in solution with DMAc and in solid phase). This compatibility, however, is not the consequence of the chemical interaction between the particles surface and the chains of the free polymer.

In fact, the formation of a chemical bond between the active substituents of the chain and the surface atoms of the particles is to be excluded: although the conditions for chemical reactivity between the imidazole groups and the atoms on the nanoparticles surface can exist, the process conditions (temperature and solvent) do not allow it. As reported elsewhere [34], this can be explained considering that the PBI chains, in solution, form structures ranging from a compact coil to an extended helical rod-like structure depending on the concentrations. Therefore, regardless of the type of interaction, these are to be excluded since the active sites of the chains (imidazole group) are engaged even when the polymer is in solution with the DMAc.

Moreover several studies presented in the literature [35, 36] show that only a suitable surface functionalization process leads to formation of bondings between nanoparticles and the imidazole group.

TGA results and activation energy

Thermogravimetric analyses were carried out on powdered samples of PBI/m and PBI/m-Z because the polymer matrix is the only reagent in the decomposition process. Samples of PBI polymer (PBI/m) and PBI polymer with nano-ZrO_2 (PBI/m-Z) were manufactured in films according to the supplier's recommendation and then reduced to powder with

Fig. 3 Dispersion of the nano-ZrO_2 particles inside a PhR-Z sample (on the left) and a PBI-Z sample (on the right)
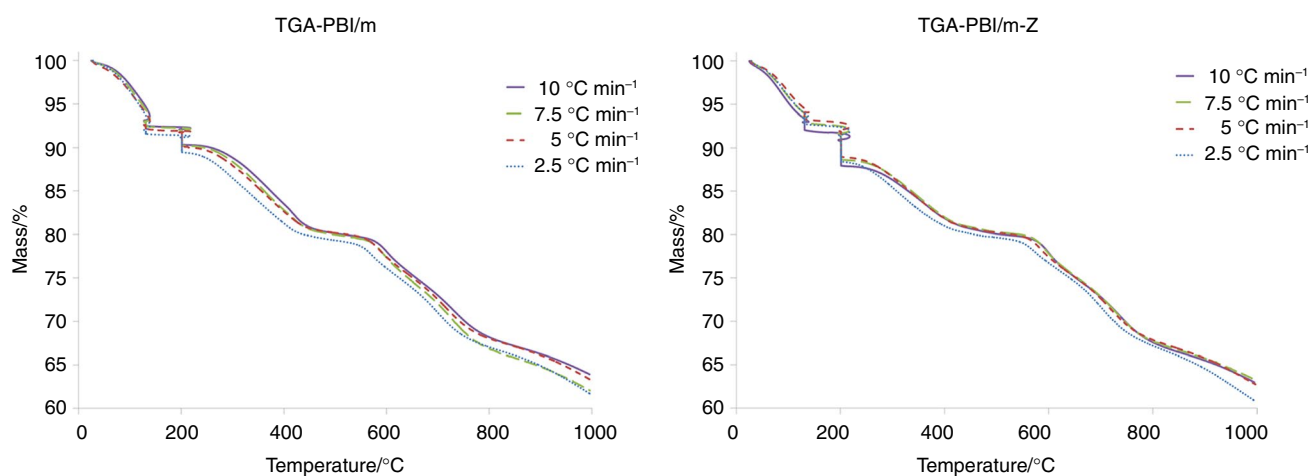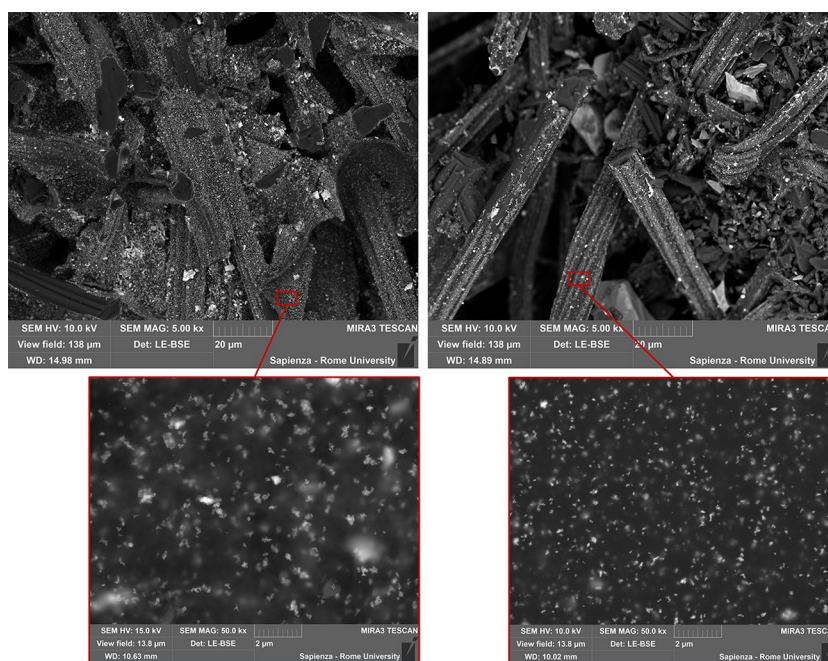

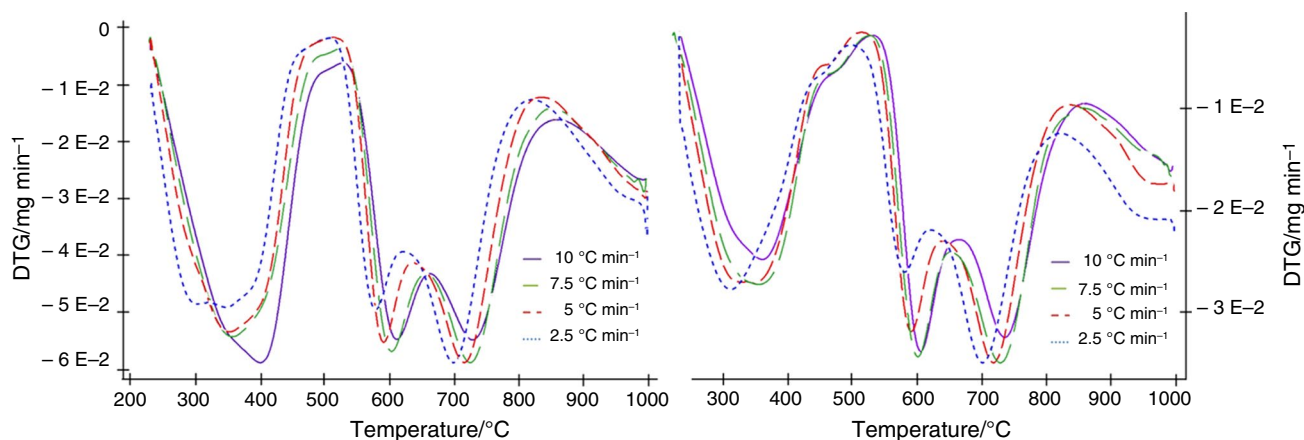**Fig. 4** TG curves for PBI samples and for PBI + nanoZrO$_2$ samples

Fig. 5 DTG curves for PBI/m (on the left) and for PBI/m-Z (on the right) samples

an agate mortar. 10 mg of powdered sample for each test was employed. For each heating rate, two tests were run to prove the reproducibility of the analysis and the curves for the same sample at the same heating rate always resulted superimposable. Furthermore, because of the hygroscopicity of the PBI, two steps of 2 h at 130 °C and 200 °C were necessary to eliminate moisture, as suggested by PBI manufacturer. For this reason, the TG curves have to be considered significant only at temperatures higher than 200 °C (Fig. 4). DTG curves are shown in Fig. 5 and show three different peaks which correspond at least to three steps of degradation with peak temperatures of about 350 °C, 600 °C and 725 °C. Even at the maximum temperature, as observed in other works [37], the TG curves do not reach a plateau, thus highlighting that the decomposition process is not complete.

Literature data show that PBI is thermally stable for temperature as high as 420 °C [38], thus the observed first step of reaction can be mainly due to the presence of residual solvent, as already reported in other works [38, 39]. This phenomenon was confirmed by the TG analyses carried out on "solvent free" PBI powders supplied by Celazole exhibiting the same behavior of the PBI/m but with a higher peak temperature for the first step, thus confirming the role of the residual solvent in the first part of the decomposition process. Iqbal et al. [40] reported the trend of TG curve for Celazole PBI under nitrogen atmosphere for an heating rate of 10 °C min⁻¹: also in this case they observed a first decrease in weight for a temperature lower than 300 °C due to the presence of solvent in the polymer. Furthermore, several literature data confirm the absence of a plateau in the TG curve for temperatures up to 1000 °C [39, 41, 42].

Each DTG curve can be approximated by the superimposition of three Gaussian functions and each of the three functions, evaluated with the AKTS software, can be considered as a single DTG curve for each single step of reaction. This procedure allows for obtaining three values of

activation energy E_a for PBI/m and for PBI/m-Z. The results of the apparent activation energy for each step of reaction are shown in Fig. 6; they are the mean values of the activation energy calculated in a range of conversion extent (α) having a correlation factor r (expressing the goodness of the isoconvertion curves interpolation) higher than 0.99. While for the first step of reaction the activation energy of samples with and without nano-fillers are very similar, in particular considering the standard deviation, for the second and third step of reaction, the activation energy is higher for the samples with nano-fillers. This phenomenon was already enlighten by other studies showing how ceramic nano-fillers can improve the thermal stability of the polymers. Jin et al. [43] studied the influence of the nano-Al₂O₃ and nano-SiC in an epoxy resin and explained how nanoparticles can increase both the glass transition temperature and the decomposition temperature of the matrix; Zabihi et al. [44] studied a nano-composite epoxy resin with ZnO as nano-filler and found an increment of thermal stability thanks to the addition of
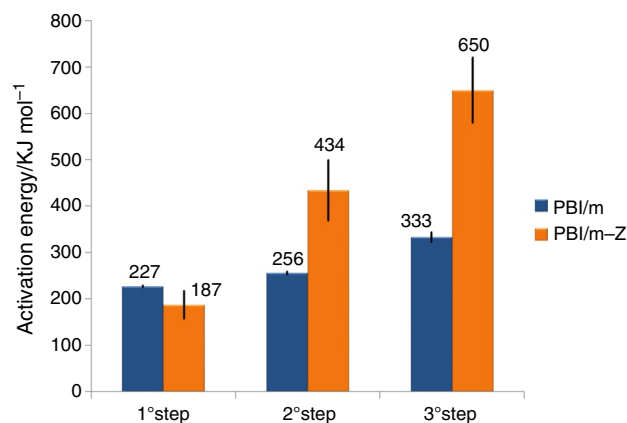

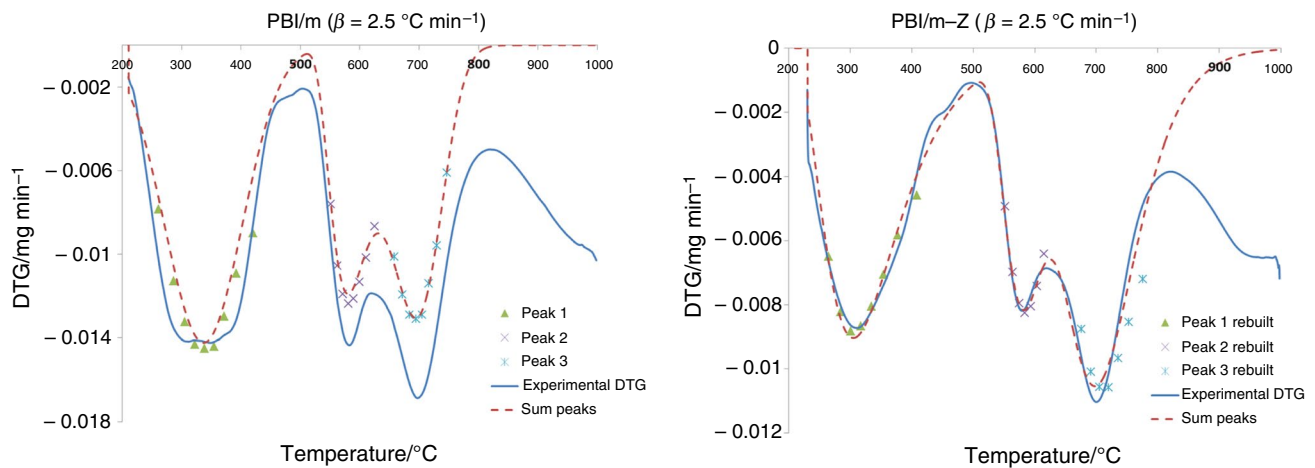**Fig. 6** Activation energy for each steps of reaction for PBI/m and PBI/m-Z

Fig. 7 Rebuilt of the experimental DTG curves with the evaluated activation energies
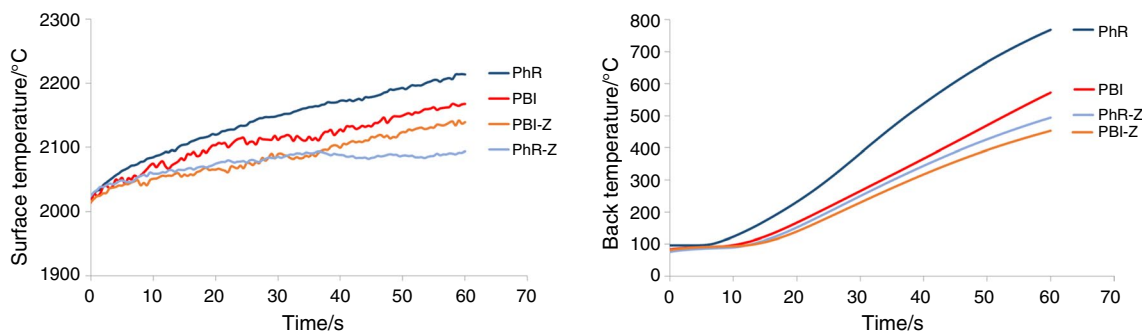

Fig. 8 Medium temperature trends for the back and surface temperature of the ablators recorded during the oxy-acetylene flame exposure

the ceramic nanoparticles with a resulting higher activation energy associated with decomposition process. In fact, when ceramic nanoparticles are added to a polymer matrix between the matrix and the fillers there is the so called interphase layer whose properties could be very different from the bulk polymer's ones. This interphase consists of flexible polymer chains, with adsorbed and unabsorbed segments, which are entangled with other chains in their proximity. The peculiar characteristics of the interface influence the properties of the composite material, for both nanocomposites and traditional composite. Anyway, thanks to the large surface area of nanoparticles, the influence of the interphase is more crucial for nanocomposites. For these reasons the nano-fillers, even if not directly involved in the degradation reaction, can influence the degradation properties [45–47].

In this work, the study of the activation energy was carried out only for PBI matrices, while an extensive study of the kinetic triplet for carbon-phenolic ablators was discussed by the authors in a previous work [48]. The results can be compared with the current study on PBI: in both cases the degradation phenomena of pyrolysis have been

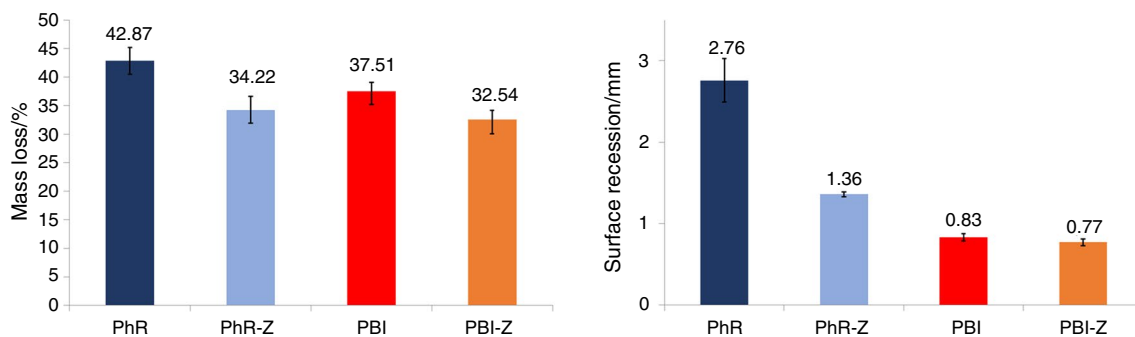**Fig. 9** Ablative material samples after the oxy-acetylene flame exposure

Fig. 10 Mass loss and surface recession of the ablative materials after the oxy-acetylene flame exposure
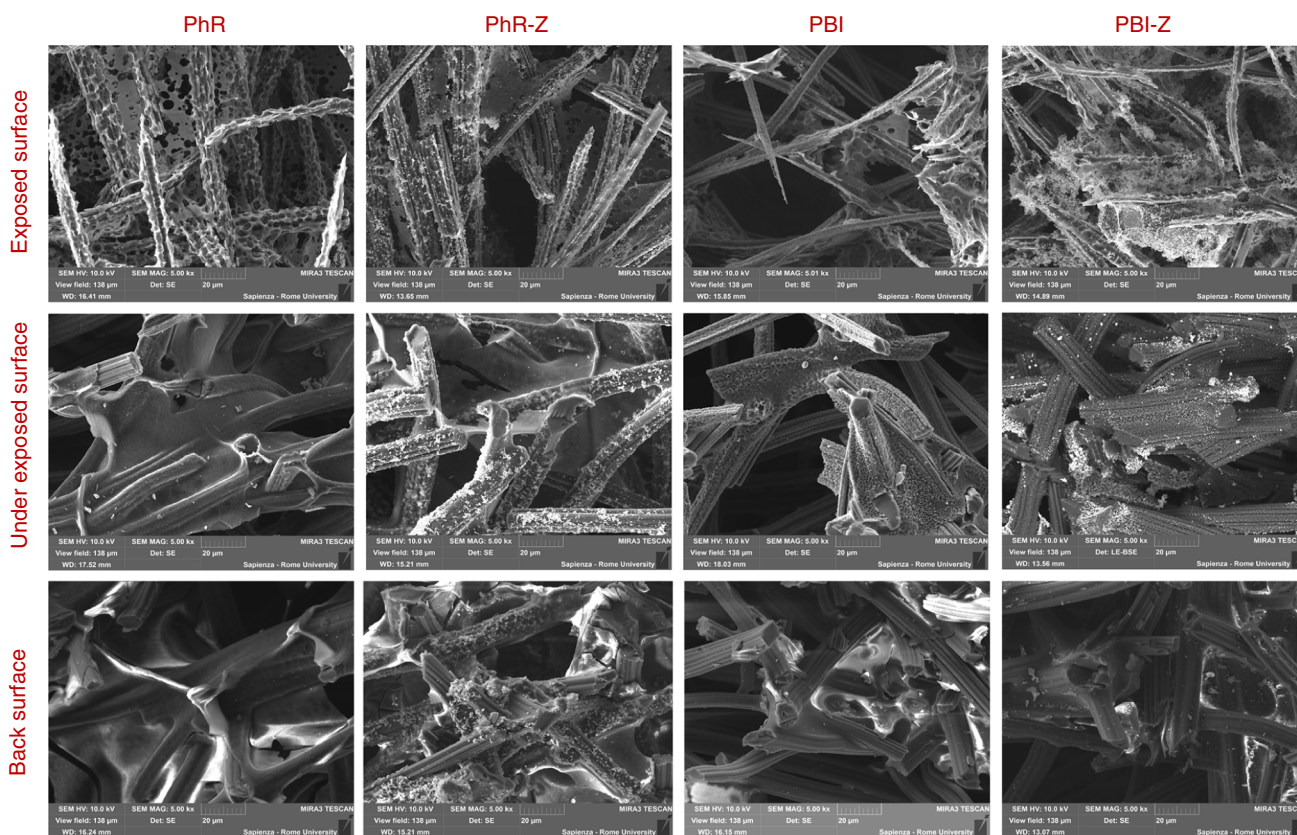

Fig. 11 SE micrographs of the samples exposed at the oxyacetylene burner

divided in three different steps of reaction. In particular, the value of activation energy for the first step is higher for PBI/m (227 ± 2 kJ mol^{-1} vs. 153 ± 16 kJ mol^{-1} for PhR), for the second peak is comparable (256 ± 2 kJ mol^{-1} vs. 256 ± 5 kJ mol^{-1}) and for the third one is still comparable (333 ± 10 kJ mol^{-1} vs. 361 ± 15 kJ mol^{-1}). The comparison between the two materials enlightens an overall higher apparent activation energy for PBI/m composite, suggesting a higher thermal stability for the PBI matrix. Furthermore, while the TG curves of the phenolic resin reach a plateau for

a temperature of about 900 °C, TG curves of PBI never reach a plateau, neither for the maximum temperature allowed by the TG facility (1400 °C). Thus, while the pyrolysis of phenolic resin ends at temperature lower than 900 °C, the PBI continues its endothermic decomposition process also at higher temperature.

The kinetics results for PBI/m and PBI/m-Z were verified by the rebuilding of the thermogravimetric curves with $\beta = 2.5$ °C min^{-1} (the lower heating rate allows for a better discrimination of the peaks). $\ln[A(\alpha(T)) \cdot f(\alpha(T))]$ and the
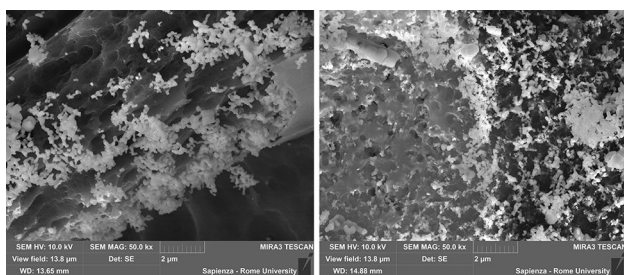
Fig. 12 Micrographs of the coalesced nanoparticles in a PhR-Z sample (on the left) and in a PBI-Z sample (on the right) due to oxyacetylene flame exposure

activation energy E_a were calculated for each step of reaction and used to rebuild the DTG curves: the results (Fig. 7) prove the reliability of the rebuilding procedure because of the good agreement in terms of position and amplitude of the peaks. After the third peak, the difference between the sum of the deconvolved peaks and experimental DTG is evident; the experimental data present a further mass decrease up to the end of the test which was not taken into account in this work for the activation energy evaluation.

Oxyacetylene flame test results

The temperature evolution measured during the oxyacetylene exposure tests on the exposed surface and on the back of the samples are reported in Fig. 8. Three samples for each kind of material were tested and the data refers to medium values. The back and the surface temperatures were reported for the effective time of testing of 60 s when the sample is exposed to a constant heat flux of 4 MW m^{-2}. A pre-heating effect is detectable in the temperature curves at the beginning of the test (time = 0 s) because of the time necessary for the approach of the torch to the test position in front of the sample. The trend of the back temperature shows that PhR ablators are less efficient if compared to the other samples: ablators manufactured with PBI are able to provide a more effective reduction of the back temperature and the addition of nano-ZrO$_2$ can improve the performance of both materials thanks to the thermal shielding effect induced by the presence of layered ZrO$_2$ nanoparticles close to the exposed surface, as already highlighted in previous works [6, 49]. In fact, the samples enriched with nano-ZrO$_2$ show a white layer on the external part of the sample hit by the heating thus exhibiting a more homogeneous recession compared to their counterpart without nano-fillers (Fig. 9). For this reason, the most promising results were obtained with PBI-Z ablators, able to guarantee the lowest back temperature during the oxyacetylene flame exposure. After the test, the samples were weighted and measured in order to estimate the mass loss and the surface recession. The results were

summarized in the graph of Fig. 10; the mass loss of PhR-Z and PBI-Z ablators was lower if compared to the PhR and PBI; moreover PBI and PBI-Z ablators show the best performance in terms of surface recession, with a reduction of about 70% with respect to PhR ablator. Thanks to all data collected during this test it is clear that the ceramic nanoparticles can improve the performance of the ablative materials. The cylindrical samples exposed to the oxyacetylene flame were cut along their main axis, and the cross sections were observed with a scanning electron microscope in Fig. 11 the micrographs show the structure of the exposed surface, the areas just under the exposed surface and an area at the back of the sample.

For the PhR and PhR-Z ablators the micrographs related to the exposed surface enlighten the different structure of the charred layer: the char on the surface of the PhR ablator is very porous and deeply consumed so that the carbon fibers are only partially covered by it. The presence of the nano-ZrO$_2$ has two different consequences; it improves the compactness of the char and, distributing along the fibers, protects the fibers themselves against phenomena of surface degradation. Just under the exposed surface, the structure of the resin is quite similar to the structure at the back of the sample showing slight decomposition phenomena: the area interested by pyrolysis is very restricted and limited to a thin layer very near to the external surface. PBI and PBI-Z micrographs of the exposed surface show a different structure of the charred layer. Although the PBI polymer is less consumed compared to the phenolic resin, the char formed because of pyrolysis reaction is less porous providing higher mechanical performance and so a less important surface recession. When nano-ZrO$_2$ is added to PBI, the structure of the char seems less porous and the nanoparticles form a layer on the carbon fiber protecting them, as in the previous case of PhR-Z ablator.

SEM micrographs about the areas under the exposed surface show a more pyrolyzed polymer compared to phenolic resin, thus the layer interested by pyrolysis is thicker. The presence of the nano-ZrO$_2$ modifies the structure of the char which results more compact. At the bottom of the sample the PBI polymer appears as in its virgin state, thus it is still not interested by evident phenomena of decomposition. The different performance of the four ablators manufactured and tested in this experimentation can be justified by the different nature of the polymer matrix, by the different distribution of the matrix inside the carbon felt and by the presence of the ceramic nano-fillers.

The different nature of the polymer matrices influences the thermal conductivity of the ablative material causing a different temperature reduction between the surface and the back of the samples. A different polymer matrix means also a different pyrolysis process: there could be difference in the char yield and in the amount and nature of the
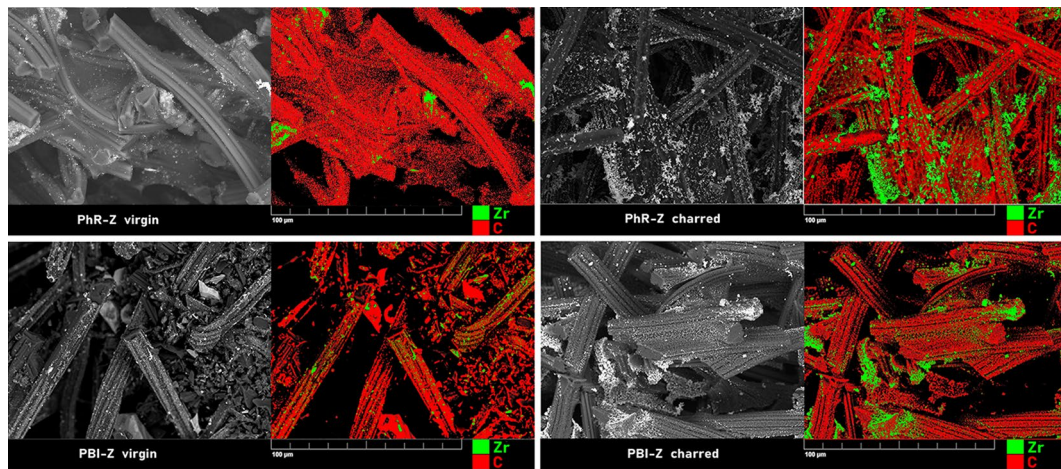
Fig. 13 EDS maps of the surface of the nano-charged samples before and after the oxyacetylene flame exposure

pyrolysis gas. This means possible variation in the quantity of energy absorbed because the endothermic reaction of pyrolysis and in the heat absorbed by the pyrolysis gas when they warm up flowing through the porous char layer. Furthermore, the physical structure of the char produced by the decomposition of the polymer can be different and can influence the recession and the mass loss [6]. The distribution of the polymer inside the carbon felt can influence the porosity of the material, the thermal conductivity and the mechanical properties. This is critical for the external charred layer which has to withstand intense shear stress causing the mechanical removal of the material.

The presence of the ceramic nano-particles can influence the structure of the char and, because of the exposure to heating flux, there could be a coalescence of nanoparticles on the surface of the ablator acting as a thermal shield hindering the heating of the material [4, 6]. This last phenomenon is enlighten in Fig. 12 showing the coalescence of nanoparticles due to exposure to the oxyacetylene flame. In Fig. 13, EDS maps of the nano-charged samples before and after the flame exposure confirm the higher agglomeration of nanoparticles after the exposure.

Conclusions

Four different light-weight ceramic ablators were manufactured using the more traditional phenolic resin or the innovative polybezimidazole as polymer matrix, a commercial carbon felt Sigratherm MFA as reinforcing phase and nanoparticles of ZrO$_2$ as a third phase. The new manufacturing processes showed to be suitable for obtaining samples with a satisfying distribution of polymer inside the carbon felt and a good dispersion of nanoparticles inside the matrix.

Thermogravimetric analysis on polymer samples were carried out at different heating rates to observe the behavior of the PBI/m and PBI/m-Z and to appreciate the difference induced by addition of nanoparticles. Three different peaks were individuated in the DTG curves, thus a three steps reaction was supposed and the three different activation energies were calculated for each material using a model-free method. Samples enriched with nanoZrO$_2$ showed higher activation energy for the second and third step of reaction, showing that the ceramic nanoparticles can act as thermal degradation stabilizer when added to PBI.

The oxyacetylene flame exposure of the four ablators confirms that PBI is a good candidate as polymer matrix in the ablative materials. PBI and PBI-Z ablators show lower back temperature, lower mass loss and surface recession. The ceramic nanoparticles selected as third phase for these ablative materials influence their performance in particular thanks to an intense phenomenon of coalescence on the exposed surface of the samples.

References

1. Bouilly JM, Dariol L, Leleu F. Ablative thermal protections for atmospheric entry. An overview of past missions and needs for future programmes. In Proceedings 5th European Workshop on Thermal Protection Systems and Hot Structures Noordwijk, The Netherlands. 2006 (ESA SP-631).

2. Pinaud G, Bertrand J, Sas AG, Mureaux L, Ritter H, Bayle O. Exomars mission, 2016: a preliminary post-flight analysis of the heat shield during entry on Mars atmosphere. AIAA SciTech Forum. 2019. https://doi.org/10.2514/6.2019-0244.

3. Pulci G, Paglia L, Genova V, Bartuli C, Valente T, Marra F. Low density ablative materials modified by nanoparticles addition: manufacturing and characterization. Compos Part A Appl Sci Manuf. 2008. https://doi.org/10.1016/j.compositesa.2018.03.025.

4. Natali M, Kenny JM, Torre L. Science and technology of polymeric ablative materials for thermal protection systems and propulsion devices: a review. Prog Mater Sci. 2016. https://doi.org/10.1016/j.pmatsci.2016.08.003.

5. Zhang J, Fang GD, Yang LW, et al. Comparison of ablative and compressive mechanical behavior of several PICA-like ablative materials. Sci China Tech Sci. 2020. https://doi.org/10.1007/s11431-020-1618-2.

6. Paglia L, Genova V, Marra F, Bracciale MP, Bartuli C, Valente T, Pulci G. Manufacturing, thermochemical characterization and ablative performance evaluation of carbon-phenolic ablative material with nano-Al_2O_3 addition. Polym Degrad Stab. 2019. https://doi.org/10.1016/j.polymdegradstab.2019.108979.

7. Bianchi D, Nasuti F, Martelli E. Navier–Stokes simulations of hypersonic flows with coupled graphite ablation. J Spacecr Rockets. 2010. https://doi.org/10.2514/1.47995.

8. Sannigrahi A, Arunbabu D, Sankar RM, Jana T. Aggregation behavior of polybenzimidazole in aprotic polar solvent. Macromolecules. 2007;40(8):2844–51.

9. Tahrim AA, Amin IN. Advancement in phosphoric acid doped polybenzimidazole membrane for high temperature PEM fuel cells: a review. J Appl Membr Sci Technol. 2019. https://doi.org/10.11113/amst.v23n1.136.

10. Faiz S, Anis A, Luqman M, Al Zahrani SM. Studies on thermal, mechanical, morphological, and viscoelastic properties of polybenzimidazole fiber reinforced high density polyethylene composites. Polym Compos. 2016;37(1):5–13.

11. Kumar S, Kumar S, Jurado-manriquez EA, Kim Y, Choi C, Baluch AH, Kim C. Polybenzimidazole (PBI) film coating for improved hypervelocity impact energy absorption for space applications. Compos Struct. 2018. https://doi.org/10.1016/j.compstruct.2017.12.052.

12. Aili D, Cleemann LN, Li Q, Jensen JO, Christensen E, Bjerrum NJ. Thermal curing of PBI membranes for high temperature PEM fuel cells. J Mater Chem. 2012. https://doi.org/10.1039/c2jm14774b.

13. Lee S, Nam KH, Seo K, Kim G, Han H. Phase inversion-induced porous polybenzimidazole fuel cell membranes: an efficient architecture for high-temperature water-free proton transport. Polymers. 2020;12(7):1604.

14. He R, Li Q, Xiao G, Bjerrum NJ. Proton conductivity of phosphoric acid doped polybenzimidazole and its composites with inorganic proton conductors. J Membr Sci. 2003. https://doi.org/10.1016/j.memsci.2003.09.002.

15. Staiti P. Proton conductive membranes based on silicotungstic acid/silica and polybenzimidazole. Mater Lett. 2001;47:241–6.

16. Paglia L, Tirillò J, Marra F, Bartuli C, Simone A, Valente T, Pulci G. Carbon-phenolic ablative materials for re-entry space vehicles: plasma wind tunnel test and finite element modeling. Mater Des. 2016. https://doi.org/10.1016/j.matdes.2015.11.066.

17. ASTM Standard E285-08 "Standard test method for oxyacetylene ablation testing of thermal insulation materials".

18. Marra F, Pulci G, Tirillo J, Bartuli C, Valente T. Numerical simulation of oxy-acetylene testing procedure of ablative materials for re-entry space vehicles. Proc Inst Mech Eng Part L J Mater Des Appl. 2011. https://doi.org/10.1177/14644207JMDA335.

19. Chem JM, Aili D, Cleemann LN, Li Q, Jensen JO, Christensen E, Bjerrum NJ. Thermal curing of PBI membranes for high temperature PEM fuel cells. J Mater Chem. 2012. https://doi.org/10.1039/c2jm14774b.

20. Rathod D, Vijay M, Islam N, Kannan R, Kharul U, Kurungot S, Pillai V. Design of an "all solid-state" supercapacitor based on phosphoric acid doped polybenzimidazole (PBI) electrolyte. J Appl Electrochem. 2009. https://doi.org/10.1007/s10800-008-9764-3.

21. Chatfield DA. Stepwise thermal degradation of polybenzimidazole foam. J Polym Sci. 1981;19:601–18.

22. Jaffe M, Menczel JD, Bessey WE. Fibers. In Turi EA (eds) Thermal characterization of polymeric materials, 2nd edn. London: Academic Press, 1997;1767–1954.

23. Li QF, Rudbeck HC, Chromik A, Jensen JO, Pan C, Steenberg T, Calverley M, Bjerrum NJ, Kerres J. Properties, degradation and high temperature fuel cell test of different types of PBI and PBI blend membranes. J Membr Sci. 2010. https://doi.org/10.1016/j.memsci.2009.10.032.

24. Vyazovkin S, Burnham AK, Criado JM, Pérez-maqueda LA, Popescu C, Sbirrazzuoli N. ICTAC Kinetics Committee recommendations for performing kinetic computations on thermal analysis data. Thermochim Acta. 2011. https://doi.org/10.1016/j.tca.2011.03.034.

25. Cui HW, Jiu JT, Sugahara T, Nagao S, Suganuma K, Uchida H, Schroder KA. Using the Friedman method to study the thermal degradation kinetics of photonically cured electrically conductive adhesives. J Therm Anal Calorim. 2015;119(1):425–33.

26. Mothe CG, de Miranda IC. Study of kinetic parameters of thermal decomposition of bagasse and sugarcane straw using Friedman and Ozawa–Flynn–Wall isoconversional methods. J Therm Anal Calorim. 2013. https://doi.org/10.1007/s10973-013-3163-7.

27. Li J, Huang J, Yinc R. Multistage kinetic analysis of DMAA/MBAM polymer removal from gelcast ceramic parts using a multistage parallel reaction model and model-free method. RSC Adv. 2019. https://doi.org/10.1039/c9ra04489b.

28. Vrandečić NS, Erceg M, Andričić B, Blanco I, Bottino FA. Characterization of poly(ethylene oxide) modified with different phenyl hepta isobutyl polyhedral oligomeric silsesquioxanes. J Therm Anal Calorim. 2020. https://doi.org/10.1007/s10973-020-10076-4.

29. AKTS-Thermokinetics v 5.31—user manual.

30. Yao F, Wu Q, Lei Y, Guo W, Xu Y. Thermal decomposition kinetics of natural fibers: activation energy with dynamic thermogravimetric analysis. Polym Degrad Stabil. 2008;93(1):90–8. https://doi.org/10.1016/j.polymdegradstab.2007.10.012.

31. Sbirrazzuoli N. Is the Friedman method applicable to transformations with temperature dependent reaction heat? Macromol Chem Phys. 2007. https://doi.org/10.1002/macp.200700100.

32. Gözke G, Açıkalın K. Pyrolysis characteristics and kinetics of sour cherry stalk and flesh via thermogravimetric analysis using isoconversional methods. J Therm Anal Calorim. 2020. https://doi.org/10.1007/s10973-020-10055-9.

33. Ptáček P, Šoukal F, Opravil T, Havlica J, Brandštetr J. The kinetic analysis of the thermal decomposition of kaolinite by DTG technique. Powder Technol. 2011. https://doi.org/10.1016/j.powtec.2010.11.035.

34. Sannigrahi A, Arunbabu D, Sankar RM, Jana T. Aggregation behavior of polybenzimidazole in aprotic polar solvent. Macromolecules. 2007. https://doi.org/10.1021/ma070049q.

35. Wang Y, Shi Z, Fang J, Xu H, Yin J. Graphene oxude/polibenzimidazole composites fabricated by a solvent-exchange method. Carbon. 2011. https://doi.org/10.1016/j.caron.2010.11.036.

36. Chang YN, Lai JY, Liu YL. Polybenzimidazole (PBI)-functionalized silica nanoparticles modified PBI nanocomposite membranes for proton exchange membranes fuel cells. J Membr Sci. 2012;1(403):1–7.

37. Escorihuela J, García-Bernabé A, Montero A, Andrio A, Sahuquillo Ó, Gimenez E, Compañ V. Proton conductivity through polybenzimidazole composite membranes containing silica nanofiber mats. Polymers. 2019. https://doi.org/10.3390/polym11071182.

38. Wang H, Wu S. Synthesis and their thermal and thermo-oxidative properties of poly(benzimidazole amide imide) copolymers. J Polym Res. 2005. https://doi.org/10.1007/s10965-004-1307-y.

39. Rhine et al. Benzimidazole based Aerogel Materials, United States Patent no. US 9,434,831 B2; 2016.

40. Iqbal HMS, Bhowmik S, Benedictus R. Durability of PBI adhesive bonded joints under various environmental conditions. Int J Adhes Adhes. 2019. https://doi.org/10.1016/j.ijadhadh.2019.01.006.

41. Tashvigh AA, Chung TS. Robust polybenzimidazole (PBI) hollow fiber membranes for organic solvent nanofiltration. J Membr Sci. 2019. https://doi.org/10.1016/j.memsci.2018.11.048.

42. Lee J, Kim K, Khan SB, Han P, Seo J, Jang W, Han H. Synthesis, characterization, and thermal and proton conductivity evaluation of 2,5-polybenzimidazole composite membranes. J Nanomater. 2014. https://doi.org/10.1155/2014/460232.

43. Jin F, Park S. Thermal properties of epoxy resin/filler hybrid composites. Polym Degrad Stab. 2012. https://doi.org/10.1016/j.polymdegradstab.2012.08.015.

44. Zabihi O, Mostafavi SM, Ravari F, Khodabandeh A, Hooshafza A, Zare K, Shahizadeh M. The effect of zinc oxide nanoparticles on thermo-physical properties of diglycidyl ether of bisphenol A/2,2-diamino-1,1-binaphthalene nanocomposites. Thermoch Acta. 2011. https://doi.org/10.1016/j.tca.2011.04.003.

45. Chang Y, Lai J, Liu Y. Polybenzimidazole (PBI)-functionalized silica nanoparticles modified PBI nanocomposite membranes for proton exchange membranes fuel cells. J Membr Sci. 2012. https://doi.org/10.1016/j.memsci.2012.01.043.

46. Ciprari D, Jacob K, Tannenbaum R, January RV, Re V, Recei M, July V. Characterization of polymer nanocomposite interphase and its impact on mechanical properties. Macromolecules. 2006. https://doi.org/10.1021/ma0602270.

47. Thomas P, Ashokbabu A, Vaish R. Structural, thermal and dielectric properties and thermal degradation kinetics of nylon 11/CaCu$_3$Ti$_4$O$_{12}$ (CCTO) nanocomposites. J Therm Anal Calorim. 2020. https://doi.org/10.1007/s10973-019-09105-8.

48. Paglia L, Genova V, Marra F, Bracciale MP, Bartuli C, Valente T, Pulci G. Manufacturing, thermochemical characterization and ablative performance evaluation of carbon-phenolic ablative material with nano-Al$_2$O$_3$ addition. Polym Degrad Stabil. 2019. https://doi.org/10.1016/j.polymdegradstab.2019.108979.

49. Pulci G, Tirillò J, Marra F, Fossati F, Bartuli C, Valente T. Carbon-phenolic ablative materials for re-entry space vehicles: manufacturing and properties. Compos Part A Appl Sci Manuf. 2010. https://doi.org/10.1016/j.compositesa.2010.06.010.